Modal Analysis of Electromagnetic Couplings between SMA-Feedthrough Electrode and Beam for Wideband Beam Monitor

Tsuyoshi Suwada

High Energy Accelerator Research Organization (KEK), SOKENDAI (The Graduate University for Advanced Studies)

Abstract

The direct simultaneous detection of electron (e-) and positron (e+) bunch signals was successfully performed for the first time by a wideband beam monitor at the e+ capture section of the SuperKEKB factory [1]. This monitor can measure a time interval between the e- and e+ bunches, their bunch lengths, bunch intensities, and transverse beam positions, depending on the phase of accelerating structures. For this purpose, a new beam monitor with wideband pickups simply using SMA feedthroughs and a wideband detection system based on a real-time oscilloscope was developed to investigate their capture process at the capture section and to maximally optimize the e+ intensity. The required specification for the new monitor is to simultaneously detect the e- and e+ bunches generated in the capture section within the resolution of pico-second level with a sufficient dynamic range in the time-interval and bunch-length measurements. In this report, the basic design and numerical results based on a modal analysis of electromagnetic couplings between the SMA-feedthrough and beam are in detail given.

Introduction

- The SuperKEKB B-factory (SKEKB) is a next generation B-factory that is currently in operation at KEK. The SKEKB is a e+e- collider with asymmetric energies; it comprises 4 GeV e+(LER) and 7 GeV e-(HER) rings.
- The requirements for the injector linac are full energy injection into the SKEKB rings with the e- and e+ bunch charges of 5 and 4 nC, respectively. The injector linac should deliver high-current e+ beams to the SKEKB rings.
- Since both the electrons and positrons with approximately equivalent amounts of bunch charges are generated at the target, not only the positrons but also the electrons are simultaneously captured and accelerated (or decelerated) in the capture section with a certain time interval that is dependent on the operational condition of the capture section.
- It is a challenging to experimentally verify and elucidate complicated beam dynamics for both positrons and electrons in the capture section in order to fully understand them and to maximize the e+ intensity under an optimized operation condition.
- For this purpose, new beam monitors with not only wideband pickups but also a wideband detection system were installed at the capture section to simultaneously detect e- and e+ signals during the summer shutdown of 2019.

Positron Capture Section
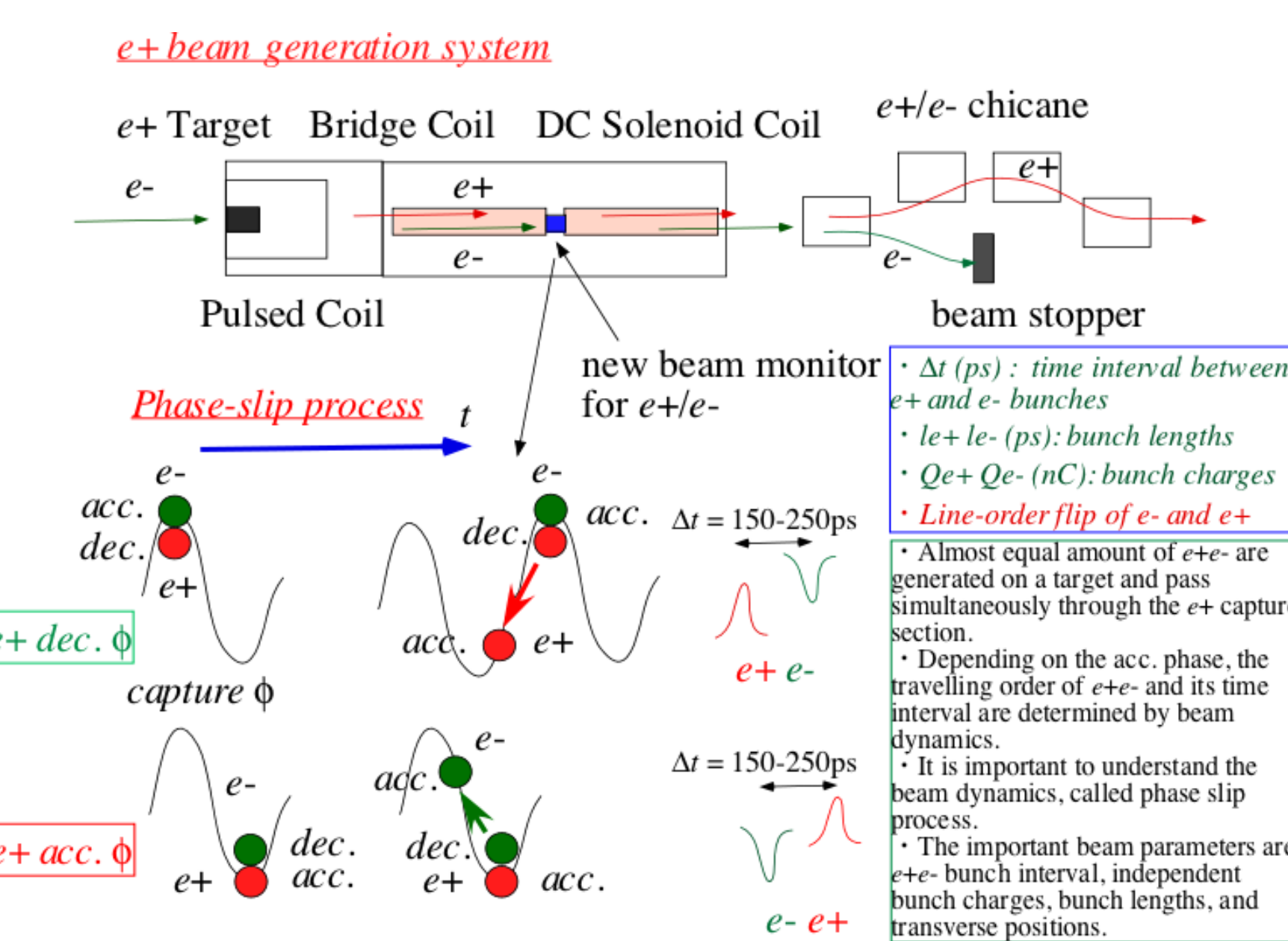
- It is difficult to simultaneously and separately measure both e- and e+ bunches at the e+ capture section due to bandwidth of its detection system.
- However, it is important to separately measure both e- and e+ bunches in order to investigate beam dynamics in their bunching process and to maximize the e+ intensity.
- The bunch interval between e- and e+ bunches spreads 150-250ps strongly depending on operation condition.
- It should be required to apply an optimization in multi-dimensional parameters, because a lot of beam and device parameters may contribute to the e+ production yield.

- Δt (ps) : time interval between e+ and e- bunches
- le + le- (ps): bunch lengths
- Qe+ Qe- (nC): bunch charges
- Line-order flip of e- and e+

- Almost equal amount of e+e- are generated on a target and pass simultaneously through the e+ capture section.
- Depending on the acc. phase, the travelling order of e+e- and its time interval are determined by beam dynamics.
- It is important to understand the beam dynamics, called phase slip process.
- The important beam parameters are e+e- bunch interval, independent bunch charges, bunch lengths, and transverse positions.

Wideband Beam Monitor System

- Fig. 1 Mechanical structure of the new BPM
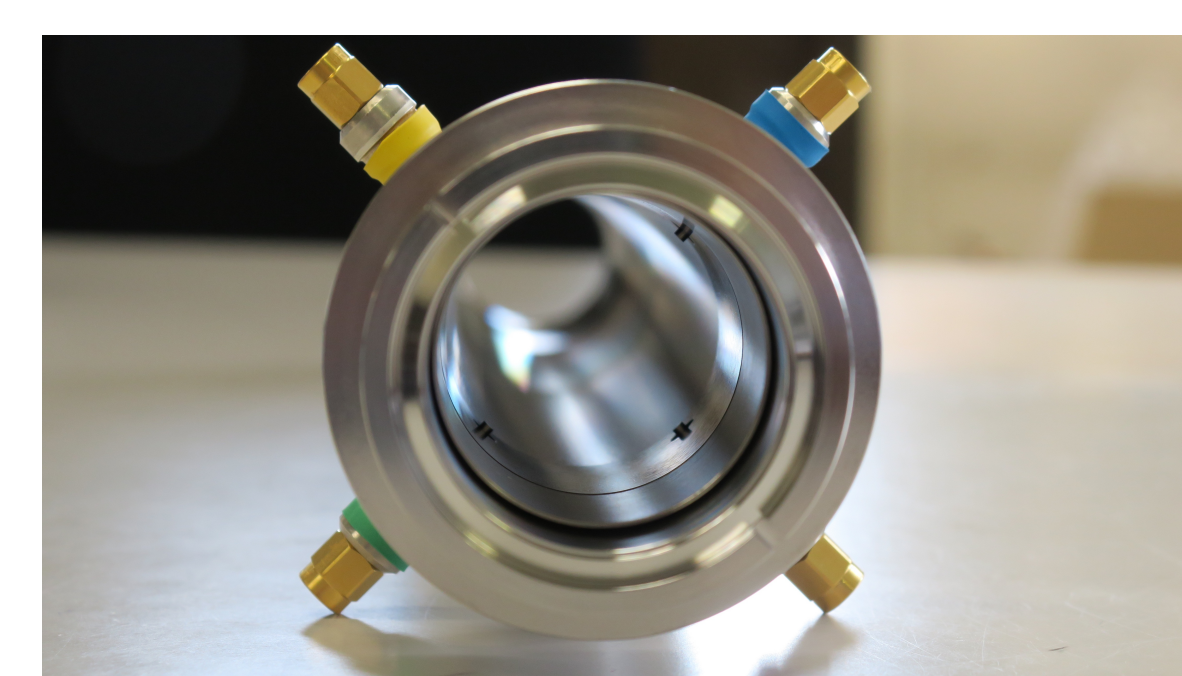
spec.	
Length	431 mm
Electrode	SMA feedthrough, 4 p.us/ 90 deg symmetry Protrusion of pin 1 mm, f_c > 10 GHz
Inner dia.	38 mm
Flange	KFS-NW40

- Fig. 2 Signal detection system

1. coax.1 (semi-rigid PEEK)
2. coax.2 (Fujikura Dia., 10D-HFB-CE)
3. coax.3 (RG-223)
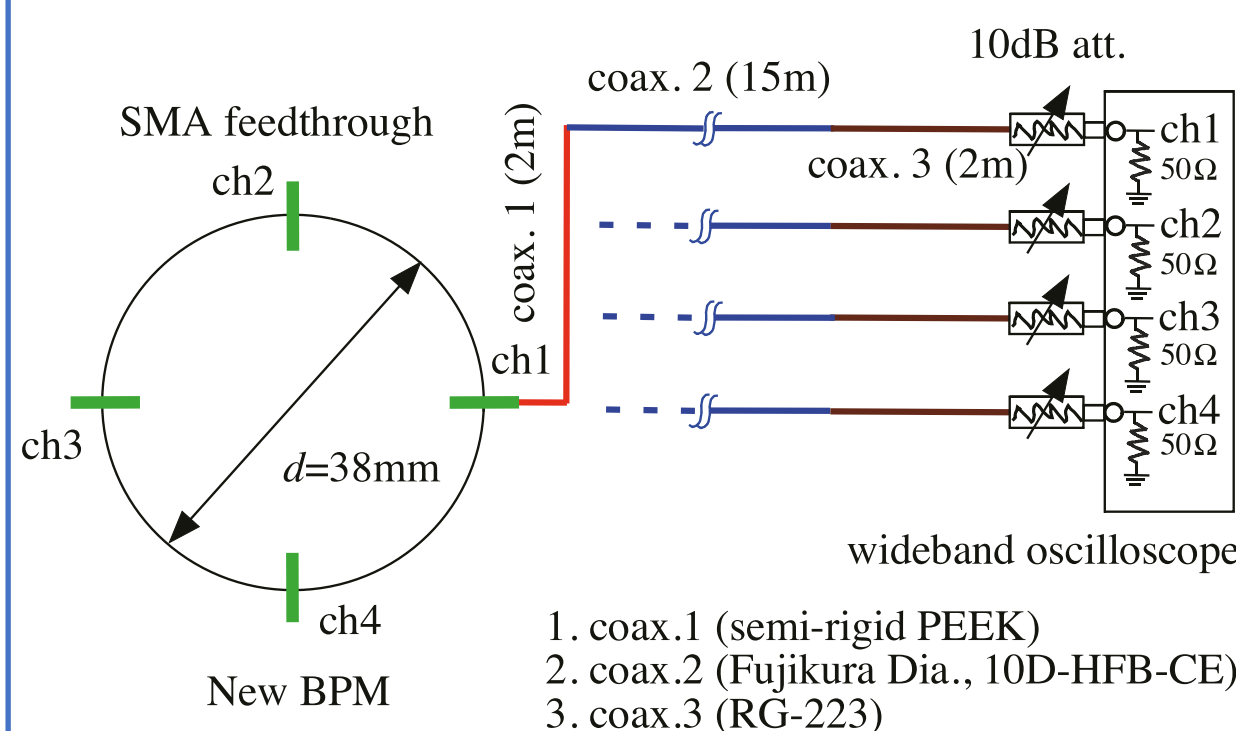
- Total length of coaxial cables should be at minimum.
- 10D coax. should be used to reduce high frequency loss as much as possible.
- However, coax. cables with larger diameter should not be used, because higher-order modes may be excited.
- Radiation-hard coax. should be used in the frontend.
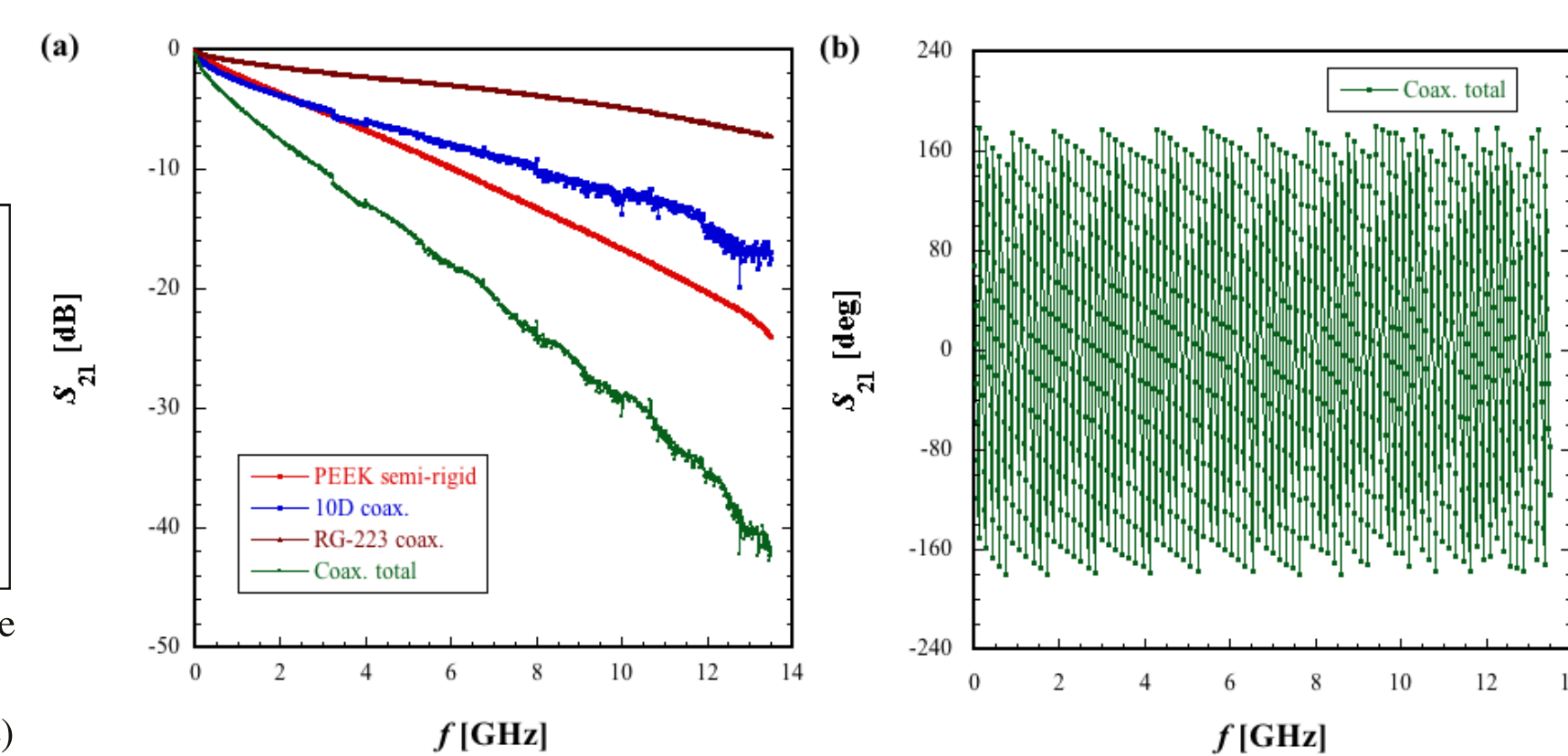
Figure 3: Measured S21 -parameters, (a) amplitude and (b) phase, of a typical coax. cable connected with three different coax. cables in series.

Electromagnetic Coupling Analysis

Detection Principles
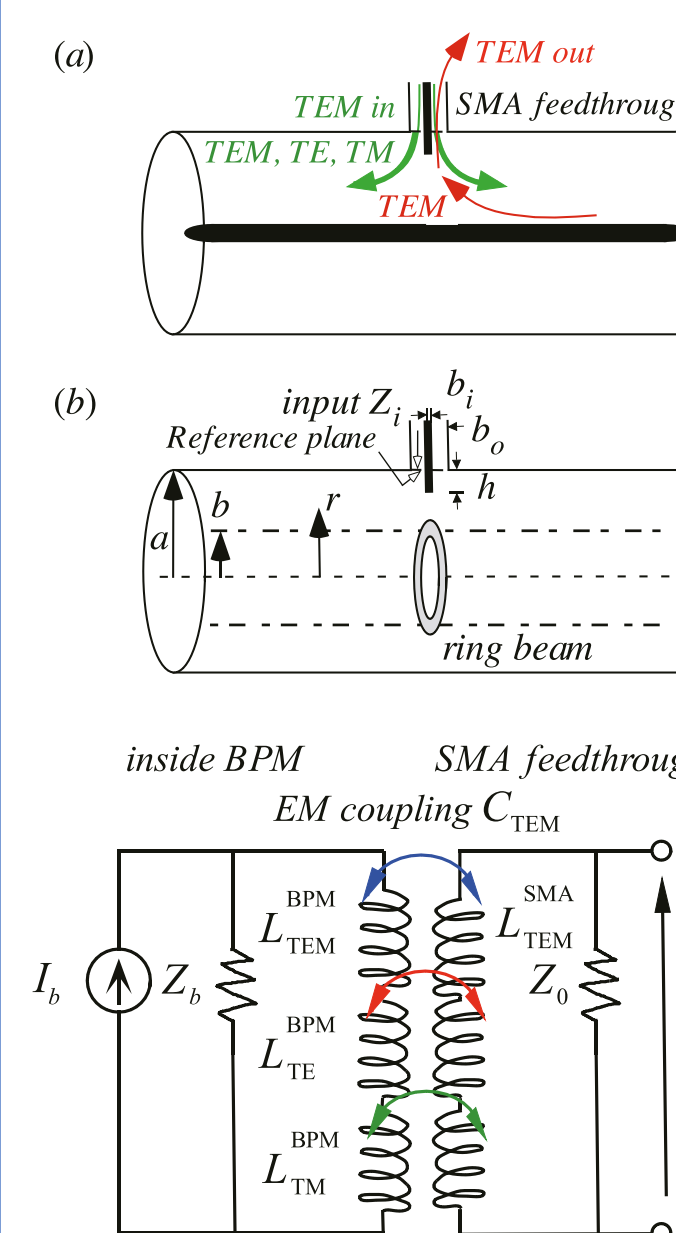
Figure 3:

(a) Schematic drawing of electromagnetic couplings between SMA feedthrough and coaxial structure.

(b) Electromagnetic couplings between SMA feedthrough and a thin ring beam. Inner radius of the coaxial structure: a = 19 mm, ring-beam radius: b, radii of the SMA inner and outer conductor: bi = 0.9 mm, bo = 2.05 mm, and the characteristic impedance of the SMA is Z_0 = 50 **Ω**.

Figure 4: Equivalent circuit of electromagnetic couplings between SMA feedthrough and coaxial structure. The arrows indicate the couplings between TEMs (blue), TE and TEM (red), and TM and TEM (green).

Analytical Formulation

If SMA feedthrough is excited by an external rf source, TEM excited in a coaxial tube is represented by (see [2])

$$E_{r_0}(r) = \frac{1}{\sqrt{\ln(a/b)}}\frac{1}{r}, \quad E_{\phi_0}(r) = 0. \quad (1)$$

The higher-order TEs are represented by

$$E_{r_{mn}}(r) = \frac{\sqrt{\pi}(m/r)[J_m(k_{cmn}r)N'_m(k_{cmn}b)-N_m(k_{cmn}r)J'_m(k_{cmn}b)]}{\sqrt{(J'_m(k_{cmn}b)/J'_m(k_{cmn}a))^2[1-(m/k_{cmn}a)^2]-[1-(m/k_{cmn}b)^2]}}, \quad (2)$$

$$E_{\phi_{mn}} = \frac{\sqrt{\pi}(k_{cmn})[J'_m(k_{cmn}r)N'_m(k_{cmn}b)-N'_m(k_{cmn}r)J'_m(k_{cmn}b)]}{\sqrt{(J'_m(k_{cmn}b)/J'_m(k_{cmn}a))^2[1-(m/k_{cmn}a)^2]-[1-(m/k_{cmn}b)^2]}}, \quad (3)$$

$$E_{r_{mn}}(\phi) = \sin(m\phi), \quad E_{\phi_{mn}}(\phi) = \cos(m\phi). \quad (4)$$

Here, E_r and E_ϕ are the excited electric fields in the radial and angular directions, respectively. The subscripts 0 and mn mean those for TEM and TE modes, respectively. $f_c(m, n)$ and k_{cmn} are the cutoff frequency and wave length for TE modes, respectively. $J_m(z)$ and $N_m(z)$ are Bessel and Neumann functions, respectively. $J'_m(z)$ and $N'_m(z)$ are derivatives on z for Bessel and Neumann functions, respectively. X'_{mn} are roots of Bessel-Nuemann combined function [?]. This relation is given by (see [3])

$$af_c(m, n) = \frac{c_0 X'_{mn}}{2\pi(b/a)}, \quad X'_{mn} = k_{cmn}b. \quad (5)$$

The input impedance Z_{in} (Z_{out}) viewed the reference plane from the SMA (BPM) side to the BPM (SMA) side can be represented by

$$Z_{in} = \frac{1}{2}\left[Z_{TEM} + \sum_{m=1}^{\infty}\sum_{n=1}^{\infty}Z_{TE_{mn}} + \sum_{m=0}^{\infty}\sum_{n=1}^{\infty}Z_{TM_{mn}}\right], \quad (3)$$

$$Z_{out} = Z_{TEM}. \quad (4)$$

Here, in eq. (3), the factor 1/2 corresponds to a junction of the excited current at the reference plane in the directions of both upstream and downstream of BPM. On the other hand, when BPM is excited in one-way direction, this factor does not need to be taken into account.

By applying these formulation, the impedances for TEM, TE and TM modes are given by

$$Z^{TEM} = \frac{\eta_0}{2\pi}\left[\int_{a-h}^{a}I(r)E_{r_0}(r)dr\right]^2, \quad (6)$$

$$Z_{mn}^{TE} = \frac{\eta_{mn}}{2\pi\sigma\int_a^b[E_{rmn}^2(r)+E_{\phi mn}^2(r)]rdr}\left[\int_{a-h}^{a}I(r)E_{rmn}(r)dr \times \int_{a-h}^{a}I(r)E_{rmn}(r)F_{mn}(r,b_i)dr\right], \quad (7)$$

$$Z_{mn}^{TM} = \frac{-jm^2\eta_{mn}}{2\pi\sigma\int_b^a r^3E_{\phi mn}^2(r)dr}\left[\int_{a-h}^{a}I(r)E_{rmn}(r)dr \times \int_{a-h}^{a}I(r)E_{rmn}(r)F_{mn}(r,b_i)dr\right]. \quad (8)$$

$$\eta_{mn} = \frac{\eta_0}{\sqrt{1-(k_{cmn}/\beta_0)^2}}, \quad \eta_0 = \sqrt{\frac{\mu_0}{\epsilon_0}} = 376.7 \, (\Omega), \quad (9)$$

$$I(r) = \frac{\sin[\beta_0(h+r-a)]}{\sin(\beta_0 h)}, \quad (10)$$

$$F_{mn}(r) = \frac{1}{2\pi}\int_0^{2\pi}e^{-\gamma mn b_i|\sin\theta|}\cos\left[m\cdot\tan^{-1}\left(\frac{b_i\cos\theta}{r}\right)\right]d\theta. \quad (11)$$

Here, h is the extruding length of the SMA feedthrough from the inner surface of BPM, η_0 the wave impedance in vacuum, η_{mn} the intrinsic impedance transmitted in BPM, β_0 the phase constant in vacuum, γ_{mn} the propagation constant of TE and TM modes, σ a constant by $\sigma = 1/2$ for $m > 0$ and $\sigma = 1$ for $m = 0$, ϵ_0 and μ_0 are permittivity and permeability in vacuum, respectively. $I(r)$ a normalized current excited in BPM, which is a function of the radius r of BPM. F_{mn} is the attenuation function of the excited electromagnetic fields in BPM as a function of r with taking into account the geometrical structure of the SMA feedthrough.

Coupling strength formula

$$C_{TEM} = \frac{Z_{out}}{Z_{BPM}}, \quad Z_{BPM} = \frac{\eta_0}{2\pi}\ln(a/b). \quad (5)$$

Numerical Results

Figure 5: (a) Variations in the input impedance (TEM and TE modes) as a function of frequency and the beam size, (b) Variations in that (TEM and TM modes) as a function of frequency and the beam size. The subscripts n and maximum m are fixed to 1 and 5, respectively. The extruding length is fixed to 1 mm.
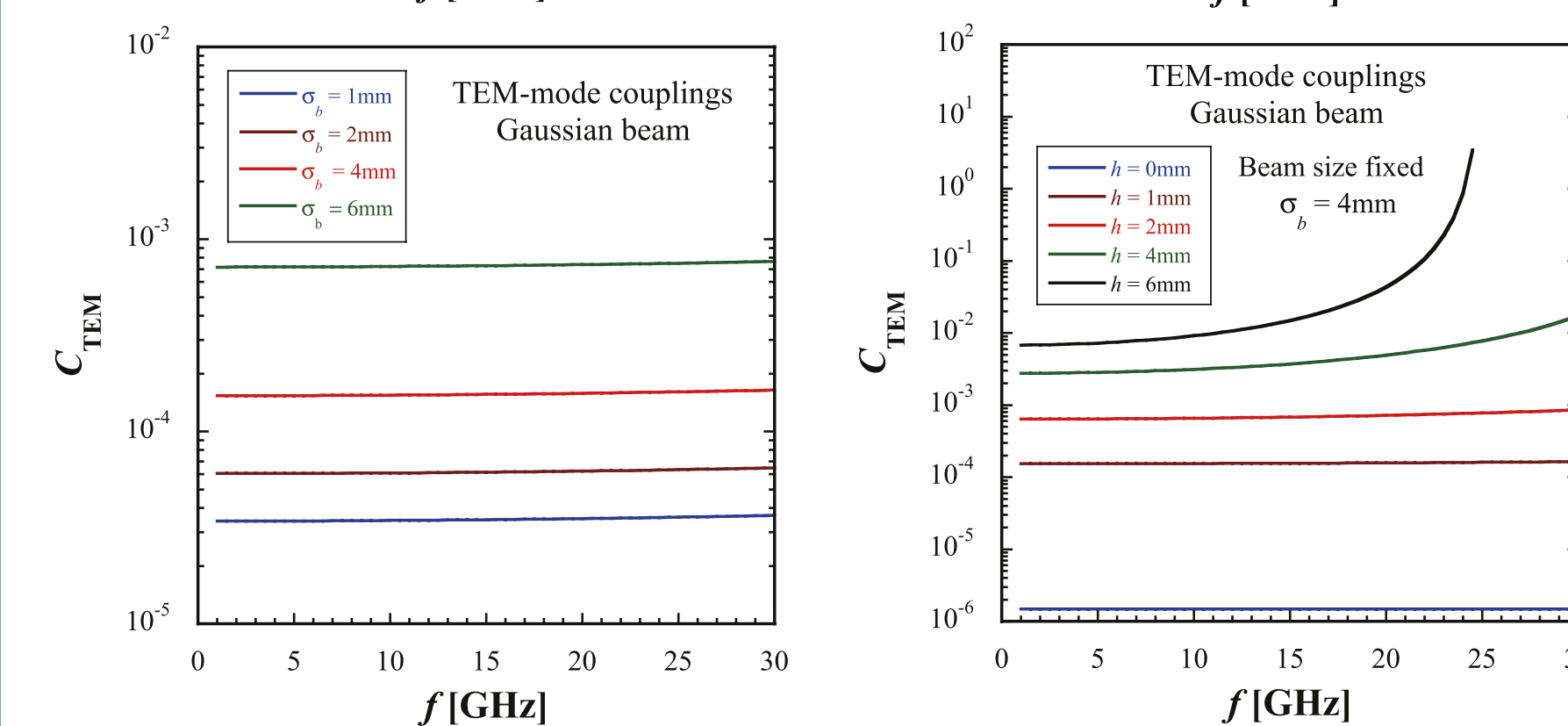
Figure 6: Variations in the coupling strengths between the TEM modes as a function of frequency and the beam size.

Figure 7: Variations in the coupling strengths between the TEM modes as functions of frequency and the length. The transverse charge distribution of σ_b = 4 mm is fixed.

- Z_{TEM} does not depend on frequency, and the higher-order modes arise in order at their corresponding cutoff frequencies starting from their lowest order.
- The input impedances of TE (TM) modes are Z_{TE} ~ 7 x10^{-3} ~ 5 x10^{-2} **Ω** (Z_{TM} ~ 7 x10^{-3} ~ 2 x10^{-2} **Ω**) depending on frequency and beam size.
- The input impedance of TE mode is larger than those of TM mode.

Conclusions

The basic design and numerical results based on a modal analysis for electromagnetic couplings between SMA-feedthrough electrode and a beam are successfully investigated.

Based on the design parameters, it was verified that the wideband monitor system can work well in the direct simultaneous detection of e- and e+ bunches.

References

[1] T. Suwada, M. A. Rehman, and F. Miyahara, Sci Rep 11, 12751 (2021). https://doi.org/10.1038/s41598-021-91707-0.
[2] J. G.Davis and A. A. P. Gibson, Int. J. Electron. 93 (5), 2006, pp. 335–346.
[3] N. Marcuvitz, Waveguide Handbook (Peter Peregrinus Ltd., UK, 1986), p. 74.